Thermal Analysis of High-Power Flip-Chip-Bonded Photodiodes

Yang Shen, John Gaskins, Xiaojun Xie, Brian M. Foley, Ramez Cheaito, Patrick E. Hopkins, and Joe C. Campbell

Abstract—**The performance of high-power photodiodes flip-chip bonded on polycrystalline aluminum nitride (AlN), single-crystal AlN, and diamond submounts are compared. The thermal boundary conductance (inverse of the thermal boundary resistance) between submount/titanium interfaces was measured and found to be the primary impedance to heat dissipation. Thermal profiles of the flip-chip-bonded devices were simulated to project the power density at failure, which is found to be inversely proportional to the diameter of the photodiodes.**

Index Terms—**Failure analysis, flip-chip devices, photodiodes, thermal conductivity.**

I. Introduction

HIGH-POWER, high-linearity photodiodes are essential components for analog optical links as they can enable high link gain, low noise figure, and high spurious free dynamic range. To achieve high RF output power at high frequency, various photodiode structures have been developed, among which the uni-traveling carrier (UTC) structure has demonstrated high saturation current at high frequency [1]–[4]. The RF output power of a UTC photodiode is generally limited by two effects: one is the space charge screening, which can cause the electric field to collapse in the depletion region and saturation of the output power [5]–[6]; the other is thermal failure [7]–[8]. Various approaches to overcome thermal restrictions have been reported [9]–[15]. Among them, flip-chip bonding to a high-thermal-conductivity heat sink has achieved the best results. In principle, a higher thermal conductivity submount material should enable higher power density at failure, which translates to higher maximum RF output power. However, the observed improvement in maximum RF output power is significantly less than would be projected based solely on the relative increase of thermal conductivities of the submounts [16]. This indicates the existence of other sources of thermal resistance within the flip-chip-bonded structure that can significantly impact device performance.

This work reports a study of three types of submounts: polycrystalline AlN (Cetek), single-crystal c-plane AlN (HexaTech), and chemical vapor deposition (CVD) grown diamond (Element Six), which have thermal conductivities of around 150, 255, 2500 W m^{-1} K^{-1}, respectively, that were measured as part of this work. Modified-UTC (MUTC) photodiodes [17], [18] were flip-chip bonded onto these submounts and their characteristics were measured. The thermal properties of the submounts were examined via time domain thermoreflectance (TDTR) measurements [19]–[24]. In addition to the thermal conductivities of the submounts, the thermal boundary conductances across the submount/Ti interfaces were also measured. Thermal boundary conductance is a measure of interface thermal resistance to thermal flow. These thermal boundary conductances were relatively constant regardless of the submount, with values ranging from ∼170 − 235 MW m^{-2} K^{-1}. This submount/Ti thermal boundary conductance, the inverse of which is the thermal boundary resistance [20], [25], [26], was identified as the thermal resistance that limits the heat dissipation of these photodiodes. Thermal profiles of the flip-chip-bonded devices were simulated with the measured thermal properties. The simulated power density at failure matches well with experimental data. A numerical approach was employed to estimate power density at failure; it was found to be inversely proportional to the diameter of the photodiodes.

II. Device Fabrication

Optical microscopy and scanning electron microscope (SEM) images of a flip-chip-bonded photodiode with submount are shown in Fig. 1(a) and (b), respectively. Fig. 1(c) is a cross sectional schematic of the photodiode-submount structure. The MUTC photodiode chip is the light rectangle in Fig. 1(a). The detailed epitaxial structure of MUTC photodiode has been described in [8]. The active area of the photodiode is a round mesa that was defined by a dry-etch process. A Ti/Pt/Au metal stack was deposited for both the p- and n-type contacts. A 250 μm-thick SiO$_2$ layer was deposited on the back of the wafer as an antireflective coating, and then the wafer was diced into 1.3 mm × 1 mm chips. The bottom section in the figures is the submount with ground-signal-ground contact pads. Gold bonding layers were plated on both the photodiode and the submount. The photodiode chips were bonded onto the submount pads using a FINEPLACER pico ma system. Most of the heat

Y. Shen, X. Xie, and J. C. Campbell are with the Department of Electrical and Computer Engineering, University of Virginia, Charlottesville, VA 22904 USA (e-mail: ys6y@virginia.edu; xx5wr@virginia.edu; jcc7s@virginia.edu).

J. Gaskins, B. M. Foley, R. Cheaito, and P. E. Hopkins are with the Department of Mechanical and Aerospace Engineering, University of Virginia, Charlottesville, VA 22904 USA (e-mail: jtg2e@virginia.edu; bmf4su@Virginia.EDU; rc3qf@virginia.edu; peh4v@virginia.edu).
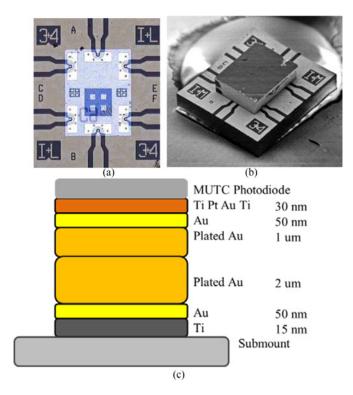
Fig. 1.   (a) Microscopic image of the photodiode flip-chip bonded on the submount. (b) SEM image of the flip-chip-bonded device. (c) Cross-sectional view of the photodiode with detail structure of metal contact layers and gold bonding layers.
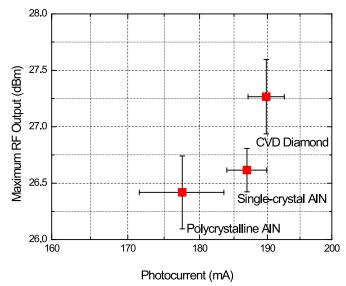

Fig. 2.   Maximum RF output power prior to failure versus photocurrent measured at 8.67 GHz for polycrystalline AlN, single-crystal AlN and CVD diamond submounts.

generated in the junction is dissipated through the metal contact, gold bonding layers, and submount. Thirty MUTC chips fabricated from the same wafer were bonded for this study. Ten devices were randomly chosen to bond with each type of submount.

III. DEVICE CHARACTERIZATION AND DISCUSSION

An optical heterodyne setup with modulation depth close to 100% was used to measure responsivity, bandwidth, and saturation characteristics. All of the devices have a diameter of $40\,\mu$m. Responsivity and dark current at -5 V were $\sim$0.6 A/W and $\sim$100 nA, respectively. For measurement of the saturation current the lensed fiber that illuminates the devices was pulled back to the position where the photocurrent dropped to half the peak photocurrent in order to maintain spatially uniform illumination. All devices under test were placed on a copper heat sink with a temperature of $\sim$20 °C. In the failure test, all of the devices were measured at 8.67 GHz. Each photodiode was first measured at a relatively low bias (-5 V) and the bias was increased. At each bias, the optical input power was gradually increased in order to achieve higher RF output power. When the device reached saturation as indicated by 1 dB compression, the highest RF output power and the corresponding average photocurrent were recorded. The bias was then increased and the procedure was repeated until the device reached thermal failure. The highest RF output powers versus photocurrent prior to thermal failure are shown in Fig. 2.

The average highest RF output power for photodiodes bonded to single-crystal AlN is slightly higher than that for the polycrystalline AlN submounts. While the average highest RF output power for CVD diamond submounts is 1.5 dB higher than the AlN devices. However, the 1.5 dB improvement in RF output power is significantly less than the order of magnitude difference in thermal conductivities between diamond and AlN.

To further examine the performance of the devices, the power conversion efficiencies for all three submounts at different biases were calculated. The total power delivered to the photodiode must equal the sum of the output power delivered by the photodiode and power dissipated in the photodiode [27], i.e.,

$$P_{Opitcal,IN} + P_{DC,IN} = P_{RF,OUT} + P_{disspated} \qquad (1)$$

$P_{Opitcal,IN}$ is the input optical power, $P_{DC,IN}$ is the electrical power delivered to the photodiode, $P_{RF,OUT}$ is the RF power delivered to the load which can be measured by an RF power meter, and $P_{dissipated}$ is dissipated heat. The ratio of the RF output power to the total input power is the power conversion efficiency, which can be expressed as

$$\eta_{PCE} = \frac{P_{RF,OUT}}{P_{Optical,IN} + P_{DC,IN}} = \frac{(m_\omega \cdot I_{ph})^2 R_{load}/2}{m_\omega \cdot I_{ph}^2 R_{load} + I_{ph}/r} \qquad (2)$$

where m_ω is the modulation depth of the fundamental RF signal, R_{load} is the load resistance. I_{ph} and r are the average photocurrent and responsivity of the photodiode, respectively. The maximum PCE equals $m_\omega/2$ when I_{ph} approaches infinity. Fig. 3 shows the power conversion efficiency of the photodiodes on the three submounts at different bias. The power conversion efficiency of the devices on the single-crystal AlN submounts is slightly better than that using the polycrystalline AlN submounts. The power conversion efficiency of the devices on CVD diamond is $\sim$5% higher than the AlN devices, which is ascribed to the fact that heat dissipates more efficiently into and through
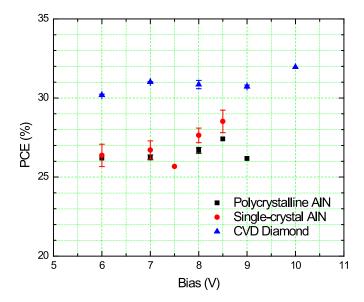
Fig. 3.   Power conversion efficiency of photodiodes on polycrystalline AlN, single-crystal AlN, and CVD diamond submounts at different bias.
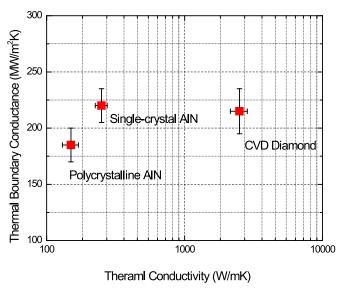

Fig. 4.   TDTR measured thermal boundary conductance versus thermal conductivity of polycrystalline AlN, single-crystal c-plane AlN, and CVD diamond submount with Ti as an adhesive layer.

the CVD diamond; we discuss this in more detail in the following section. Thus the devices on CVD diamond achieve higher photocurrent before thermal failure, and a higher photocurrent directly relates to higher power conversion efficiency.

IV. CHARACTERIZATION OF THERMAL PROPERTIES AND DISCUSSION

The thermal failure characteristics are related to the type of submount. However, there is an additional consideration, the commonly neglected thermal boundary resistance between the submounts and the Ti metal layer. Titanium serves as an adhesive layer between the gold bonding layer and the submount. TDTR measurements were performed to measure the thermal conductivity of the three submount materials and the thermal boundary conductance (the inverse of the thermal boundary resistance) of the submount/Ti interfaces. A detailed description of TDTR and the method used to extract thermal resistance values can be found in [20], [22]–[25]. The measured thermal conductivities of polycrystalline AlN, single-crystal c-plane AlN, and CVD diamond and the submount/Ti thermal boundary conductances were showed in Fig. 4.

The corresponding thermal resistance associated with the submount/Ti interface is orders of magnitude larger than the resistances associated with the metal stack and the isolated submount layer. For example, the thermal resistance at these submount/Ti interfaces functions the same as a $\sim$7 nm layer of amorphous SiO_2 (an equivalent thermal resistance of $\sim$5 m^2 K GW^{-1}). This results in a thermal bottle neck that limits the heat dissipation of the photodiodes.

A 3-D thermal model of the flip-chip-bonded devices based on the finite-element simulator COMSOL Multiphysics was created to project the power density at failure. The measured thermal boundary conductance and thermal conductivity of the submounts were incorporated into the model. It was assumed that the devices failed at a common core temperature of 470 K
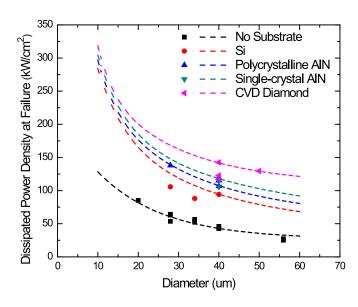

Fig. 5.   Measured (symbols) and simulated (dashed lines) dissipated power density at failure compared versus device diameter.

[8]. The power density at failure was projected for bare photodiodes without flip-chip bonding and for photodiodes bonded to Si, polycrystalline AlN, single-crystal c-plane AlN, and CVD diamond submounts. The simulations are shown as dashed lines in Fig. 5. The dots in Fig. 5 are the measured power densities at failure for these submount configurations [10]–[15]. The thermal model fits well with the experimental results.

One can also observe that the smaller devices have higher power density at failure. To explain this, a simple model was developed to investigate the relationship between device diameter and the power density at failure. The photodiode is modeled as a circular heat source having radius, a, and the submount with thermal conductivity, k, can be assumed to be much larger than the heat source as illustrated in Fig. 6, i.e., $b \gg a$. A
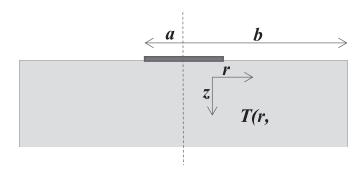
Fig. 6. Model for dissipated power density at failure.

steady-state problem can be defined and the temperature field is two-dimensional in circular coordinates, $T(r, z)$.

The mixed-boundary conditions on the top surface are:

$$z = 0, a > r > 0, T = T_o \tag{3}$$

$$z = 0, r > a, \frac{\partial T}{\partial z} = 0 \tag{4}$$

The total heat flow from the isothermal circular source into the heat sink can be expressed as [28]:

$$Q = \iint_s \frac{\partial T}{\partial Z} 2\pi r \cdot k \cdot dr \tag{5}$$

$$Q = \int_0^a -k \cdot 2\pi r \cdot \frac{\partial T}{\partial Z} dr \tag{6}$$

$$Q = 4kaT_0 \tag{7}$$

It follows that the total heat power density per unit area of the heat source is

$$P_{density} = \frac{4kaT_o}{\pi a^2} = \frac{4kT_o}{\pi a} \tag{8}$$

The calculated power density at failure via this simple 2-D model is inversely proportional to the diameter of the photodiodes. This explains the trend that smaller devices have higher power density at failure as shown in Fig. 5.

V. CONCLUSION

In conclusion, the thermal performance of MUTC photodiodes mounted on single-crystal AlN is slightly better than those on polycrystalline AlN. The average highest RF output power of photodiodes bonded to CVD diamond is 1.5 dB higher than those on AlN. The improvement in RF output power is significantly less than the relative difference of thermal conductivities of diamond and AlN. Thermal boundary resistance between the submount and the Ti layer was found to be the heat dissipation bottleneck.

REFERENCES

[1] A. Beling, A. S. Cross, Q. Zhou, Y. Fu, and J. C. Campbell, "High-power flip-chip balanced photodetector with >40 GHz bandwidth," in *IEEE Photon. Conf.*, 2013, pp. 352–353.

[2] S. Cross, Q. Zhou, A. Beling, Y. Fu, and J. C. Campbell, "High-power flip-chip mounted photodiode array," *Opt. Express*, vol. 21, pp. 9967–9973, 2013.

[3] K. Sakai, E. Ishimura, M. Nakaji, S. Itakura, Y. Hirano, and T. Aoyagi, "High-current back-illuminated partially depleted-absorber p-i-n photodiode with depleted nonabsorbing region," *IEEE Trans. Microw. Theory Techn.*, vol. 58, no. 11, pp. 3154–3160, Nov. 2010.

[4] Q. Zhou, A. S. Cross, F. Yang, A. Beling, and J. C. Campbell, "Development of narrowband modified uni-travelling-carrier photodiodes with high power efficiency," in *Proc. IEEE Avionics, Fiber-Opt. Photon. Conf.*, 2013, pp. 65–66.

[5] K. J. Williams and R. D. Esman, "Design considerations for high current photodetectors," *J. Lightw. Technol.*, vol. 17, no. 8, pp. 1443–1454, Aug. 1999.

[6] K. J. Williams, R. D. Esman, and M. Dagenais, "Effects of high space-charge fields on the response of microwave photodetectors," *IEEE Photon. Technol. Lett.*, vol. 6, no. 5, pp. 639–641, May 1994.

[7] H. Pan, A. Beling, H. Chen, and J. C. Campbell, "The frequency behavior of the intermodulation distortions of modified uni-traveling carrier photodiodes based on modulated voltage measurements," *IEEE J. Quantum Electron.*, vol. 45, no. 3, pp. 273–277, 2009.

[8] A. Beling, X. Xie, and J. C. Campbell, "High-power, high-linearity photodiodes," *Optica*, vol. 3, pp. 328–338, 2016.

[9] D. A. Tulchinsky, X. Li, N. Li, S. Demiguel, J. C. Campbell, and K. J. Williams, "High-saturation current wide-bandwidth photodetectors," *IEEE J. Sel. Topics Quantum Electron.*, vol. 10, no. 4, pp. 702–708, Jul./Aug. 2004.

[10] Q. Zhou, A. S. Cross, F. Yang, A. Beling, and J. C. Campbell, "High-power high-bandwidth flip-chip bonded modified unitraveling carrier photodiodes," in *IEEE Photon. Conf.*, 2012, pp. 306–307.

[11] Q. Zhou, A. S. Cross, A. Beling, Y. Fu, Z. W. Lu, and J. C. Campbell, "High-power V-band InGaAs/InP photodiodes," *IEEE Photon. Technol. Lett.*, vol. 25, no. 10, pp. 907–909, May 2013.

[12] Z. Li *et al.*, "High-power high-linearity flip-chip bonded modified uni-traveling carrier photodiode," *Opt. Express*, vol. 19, pp. B385–B390, 2011.

[13] Z. Li, H. P. Pan, H. Chen, A. Beling, and J. C. Campbell, "High saturation-current modified uni-traveling-carrier photodiode with cliff layer," *IEEE J. Quantum Electron.*, vol. 46, no. 5, pp. 626–632, May 2010.

[14] Q. Zhou *et al.*, "Balanced InP/InGaAs photodiodes with 1.5-W output power," *IEEE Photon. J.*, vol. 5, no. 3, Jun. 2013, Art. no. 6800307.

[15] X. Xie *et al.*, "Improved power conversion efficiency in high-performance photodiodes by flip-chip bonding on diamond," *Optica*, vol. 1, pp. 429–435, 2014.

[16] N. Duan, X. Wang, N. Li, D. Liu, and J. C. Campbell, "Thermal analysis of high-power InGaAs–InP photodiodes," *IEEE J. Quantum Electron.*, vol. 42, no. 12, pp. 1255–1258, Dec. 2006.

[17] X. Wang, N. Duan, H. Chen, and J. C. Campbell, "InGaAs-InP photodiodes with high responsivity and high saturation power," *IEEE Photon. Technol. Lett.*, vol. 19, no. 16, pp. 1272–1274, Aug. 2007.

[18] Z. Li *et al.*, "High-power high-linearity flip-chip bonded modified uni-traveling carrier photodiode," *Opt. Express*, vol. 19, no. 26, pp. B385–B390, 2011.

[19] D. G. Cahill, "Thermal conductivity measurement from 30 to 750 K: the 3w method," *Rev. Sci. Instrum.*, vol. 61, pp. 802–808, 1990.

[20] P. E. Hopkins, "Thermal transport across solid interfaces with nanoscale imperfections: Effects of roughness, disorder, dislocations, and bonding on thermal boundary conductance," *ISRN Mech. Eng.*, vol. 2013, 2013, Art. no. 682586.

[21] E. T. Swartz and R. O. Pohl, "Thermal boundary resistance," *Rev. Mod. Phys.*, vol. 61, pp. 605–668, 1989.

[22] P. E. Hopkins *et al.*, "Effect of dislocation density on thermal boundary conductance across GaSb/GaAs interfaces," *Appl. Phys. Lett.*, vol. 98, 2011, Art. no. 161913.

[23] J. C. Duda, P. E. Hopkins, Y. Shen, and M. C. Gupta, "Exceptionally low thermal conductivities of films of the fullerene derivative PCBM," *Phys. Rev. Lett.*, vol. 110, 2013, Art. no. 015902.

[24] P. E. Hopkins, J. C. Duda, C. W. Petz, and J. A. Floro, "Controlling thermal conductance through quantum dot roughening at interfaces," *Phys. Rev. B*, vol. 84, 2011, Art. no. 035438.

[25] E. T. Swartz and R. O. Pohl, "Thermal boundary resistance," *Rev. Mod. Phys.*, vol. 61, no. 3, pp. 605–668, 1989.

[26] C. Monachon, L. Weber, and C. Dames, "Thermal boundary conductance: A materials science perspective," *Annu. Rev. Mater. Res.*, vol. 46, pp. 433–463, 2016.

[27] U. Gliese, K. Colladay, A. S. Hastings, D. A. Tulchinsky, V. J. Urick, and K. J. Williams, "53.5% photodiode RF power conversion efficiency," in *Proc. Nat. Fiber Opt. Eng. Conf.*, 2010, paper PDPA7.

[28] H. S. Carslaw and J. C. Jaeger, *Conduction of Heat in Solids*. Oxford, U.K.: Clarendon, 1959.

Yang Shen received the B.S. degree in physics from the University of Science and Technology of China, Chengdu, China, in 2007, and the Ph.D. degree in electrical engineering from the University of Virginia, Charlottesville, VA, USA, in 2013. He is currently a Research Associate in the Department of Electrical and Computer Engineering, University of Virginia. His research interests include the design, fabrication, and characterization of high power and high linearity photodiodes especially the thermal management of high power photodiodes.

John Gaskins received the B.S. degree in civil engineering, the M.E. degree in mechanical and aerospace engineering, and the Ph.D. degree in mechanical and aerospace engineering from the University of Virginia, Charlottesville, VA, USA, in 2013. His Ph.D. focused experimental methods and analytical solutions used to determine elastic-plastic properties of sub-micron thin films via indentation testing of microfabricated structures. He is currently a Senior Scientist in the ExSiTE group, Charlottesville, VA, USA, focusing on thermal transport in composites at high temperatures and thermal mitigation of high power, high frequency devices.

Xiaojun Xie received the B.S. degree in optical information science and technology from the University of Electronic Science and Technology of China, Chengdu, China, in 2010, the M.S. degree in electromagnetic field and microwave technology from the Beijing University of Posts and Telecommunications, Beijing, China, in 2013, and the Ph.D. degree in electrical engineering from the University of Virginia, Charlottesville, VA, USA. He is currently a Senior Hardware Engineer at the Infinera Corporation, Sunnyvale, CA, USA.

Brian M. Foley received the B.E. and M.S. degrees in electrical & computer engineering from Worcester Polytechnic Institute, Worcester, MA, in 2007 and 2009, respectively, where he focused on nondestructive evaluation technologies for General Motors. Prior to entering the PhD program at the University of Virginia, Diodes, Inc., Charlottesville, VA, USA, making vector network analyzer extension modules for calibrated S-parameter measurements from 75 to 1100 GHz.

Ramez Cheaito received the B.S. degree in physics from the Faculty of Sciences, Lebanese University, Beirut, Lebanon, in 2008, the Ph.D. degree in mechanical and aerospace engineering from the University of Virginia, Charlottesville, VA, USA, in August 2015. His Ph.D. focused on size effects in the electron and phonon thermal conductivity of alloy and superlattice thin films. He then worked for two years as a Research Assistant in the Masdar Institute of Science and Technology, Abu Dhabi, UAE. He is currently a Postdoctoral scholar focusing on novel pump-probe measurements of thermal transport in thin films.

Patrick E. Hopkins received the Ph.D. degree in mechanical and aerospace engineering from the University of Virginia in 2008, following a B.S. in Mechanical Engineering and a B.A. in Physics at UVA in 2004. He is an Associate Professor in the Department of Mechanical and Aerospace Engineering at UVA. He spent three years as a Harry S. Truman Postdoctoral Fellow at the Sandia National Laboratories in Albuquerque, NM, USA, from 2008 to 2011. He began his faculty appointment at UVA in December of 2011 as an Assistant Professor, and was promoted to an Associate Professor with tenure in August of 2015. He received the AFOSR and ONR Young Investigator Awards.

Joe C. Campbell (F'90) received the Ph.D. degree in physics from the University of Illinois at Urbana–Champaign, Champaign, IL, USA. Following graduate school, he worked at AT&T Bell Laboratories for 13 years. In January of 1989, he joined the faculty of the University of Texas as a Cockrell Family Regents Chair in Engineering. In January of 2006, he moved to the University of Virginia as the Lucian Carr Professor of Electrical and Computer Engineering. He has coauthored seven book chapters, more than 430 articles for refereed technical journals, and more than 400 conference presentations. He received several awards including the National Academy of Engineering, the IEEE Photonics Award, the OSA/IEEE LEOS John Tyndall Award, the International Symposium on Compound Semiconductors Quantum Device Award, the Heinrich Welker Medal, the OSA Nicholas Holonyak Award, and the IEEE/LEOS William Streifer Scientific Achievement Award. He is a Fellow of Optical Society of America and American Physical Society.